AD-A032 442 ROCKWELL INTERNATIONAL THOUSAND OAKS CALIF SCIENCE --ETC F/G 13/8
FUNDAMENTALS OF PLASMA ARC WELDING.(U)
OCT 76 C B SHAW, B I DAVIS, D W TROVER N00014-75-C-0789
UNCLASSIFIED SC5031.7AR NL

1 OF 1
AD A032442

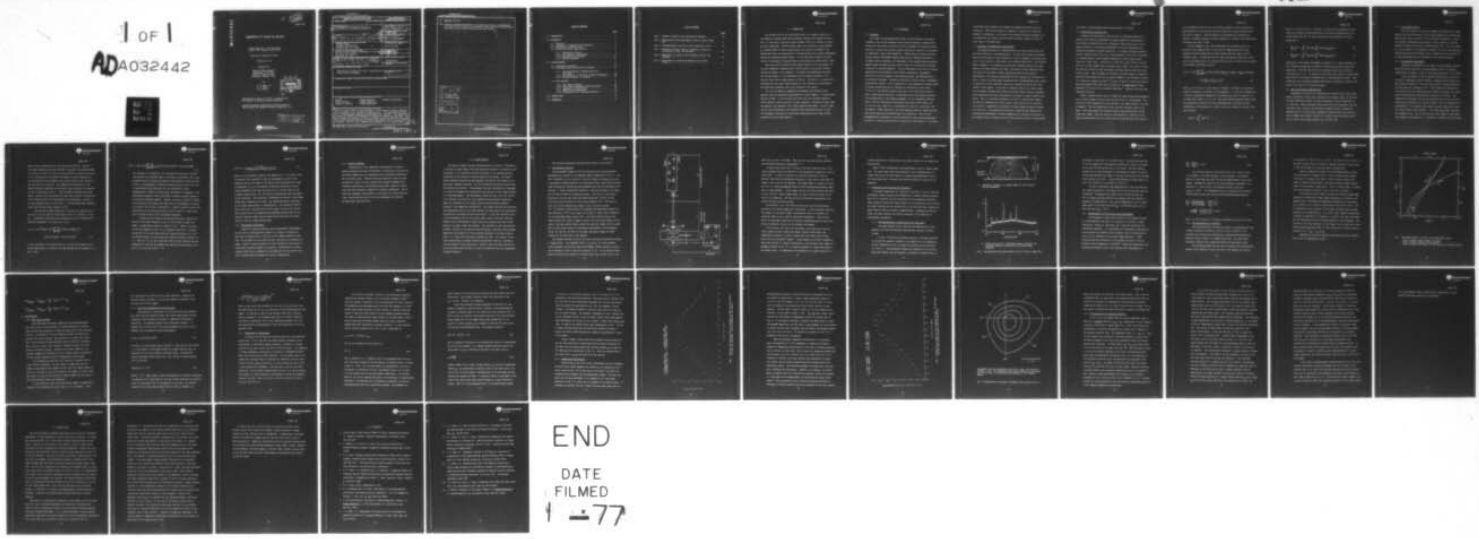

END

DATE FILMED
1-77

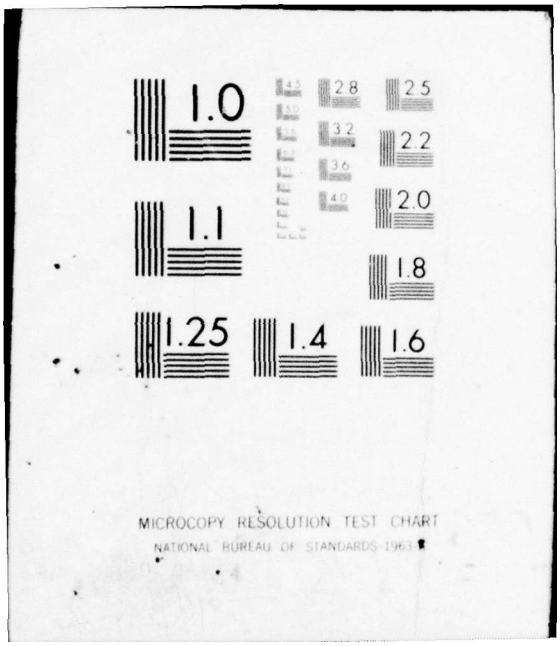
1.0
1.1
1.25
1.4
1.6
1.8
2.0
2.2
2.5
2.8
3.2
3.6
4.0
MICROCOPY RESOLUTION TEST CHART
NATIONAL BUREAU OF STANDARDS 1963

FG (12)

SC5031.7AR

FUNDAMENTALS OF PLASMA ARC WELDING

Annual Report No. 1 for the Period
1 April 1975 through 31 March 1976

Contract No. N00014-75-C-0789

Project No. 471

Prepared for

Office of Naval Research
Department of the Navy
800 North Quincy Street
Arlington, Virginia 22217

by

C. B. Shaw, Jr.
B. I. Davis
D. W. Trover

Research sponsored by the Office of Naval Research
under Contract No. N00014-75-C-0789 (Project No. 471)

Science Center
Rockwell International

Unclassified

SECURITY CLASSIFICATION OF THIS PAGE (When Data Entered)

REPORT DOCUMENTATION PAGE

READ INSTRUCTIONS BEFORE COMPLETING FORM

1. REPORT NUMBER

2. GOVT ACCESSION NO.

3. RECIPIENT'S CATALOG NUMBER

4. TITLE (and Subtitle)
(6) Fundamentals of Plasma Arc Welding.

5. TYPE OF REPORT & PERIOD COVERED
Annual Report. no. 1
April 1, 1975-March 31, 1976

6. PERFORMING ORG. REPORT NUMBER
(14) SC5031.7AR

7. AUTHOR(s)
(10) C. B./Shaw, Jr., B. I./Davis, D. W./Trover

8. CONTRACT OR GRANT NUMBER(s)
(15) N00014-75-C-0789 NEW

9. PERFORMING ORGANIZATION NAME AND ADDRESS
Science Center
Rockwell International
Thousand Oaks, CA 91360

10. PROGRAM ELEMENT, PROJECT, TASK AREA & WORK UNIT NUMBERS
Project No. 471

11. CONTROLLING OFFICE NAME AND ADDRESS
Office of Naval Research; Department of the Navy
800 North Quincy Street
Arlington, VA 22217

12. REPORT DATE
(11) Oct[illegible] 1976

13. NUMBER OF PAGES
44

14. MONITORING AGENCY NAME & ADDRESS(if different from Controlling Office)
(9) Annual rept. no. 1,
1 Apr 75 - 31 Mar 76,
(12) 45p.

15. SECURITY CLASS. (of this report)
Unclassified

15a. DECLASSIFICATION/DOWNGRADING SCHEDULE

16. DISTRIBUTION STATEMENT (of this Report)

Reproduction in whole or in part is permitted for any purpose of the United States Government

DISTRIBUTION STATEMENT A
Approved for public release;
Distribution Unlimited

17. DISTRIBUTION STATEMENT (of the abstract entered in Block 20, if different from Report)

18. SUPPLEMENTARY NOTES

19. KEY WORDS (Continue on reverse side if necessary and identify by block number)

Welding
Fusion welding
Plasma arc welding
Plasma (physics)
Plasma diagnostics
Plasma temperature
Emission spectroscopy

20. ABSTRACT (Continue on reverse side if necessary and identify by block number)

This new project seeks to aid development of the plasma-arc welding (PAW) process by studying it as a problem in applied physics. The importance and difficulty of welding-plasma temperature measurements are indicated. New experimental and analytical methods for measurement of asymmetric plasmas are described. Continuum radiation is reported to be much stronger relative to spectral line radiation for small-standoff PAW than for either long-standoff PAW or for gas tungsten arc-welding. This can impair temperature measurement by the two-wavelength

(over) → next page

DD FORM 1 JAN 73 1473 EDITION OF 1 NOV 65 IS OBSOLETE

Unclassified

SECURITY CLASSIFICATION OF THIS PAGE (When Data Entered)

389949 AB

20. Abstract (Cont'd)

method of emission spectroscopy, but plans are given for circumventing the difficulty and correlating systematic plasma temperature-distribution measurements with welding parameters and weld quality.

TABLE OF CONTENTS

LIST OF FIGURES

1.0 INTRODUCTION

The ultimate goal of the work reported here is to improve control over the plasma-arc welding (PAW) process through rational torch design and operation, in order that it may best create reliable joints in a variety of metals and joint geometries. PAW has already shown its superiority to gas tungsten-arc welding (GTAW) in various applications, and research at Rockwell[1] has demonstrated that weld penetration in the PAW process can be pushed considerably beyond the presently-accepted limits. It now holds great promise for fabrication of heavy-section titanium alloys in hydrofoils and surface-effect ships.

This first year of study has been largely devoted to the development of accurate diagnostic techniques which reveal details of the energy transfer through the plasma to the workpiece. In essence, the temperature distribution in the plasma is to be determined from the relative intensity of two spectral lines from a single species in the arc. The ability to perform this determination rests upon recent advances at this laboratory in experimental and analytical techniques, which are reviewed in this report.

The two-line method of temperature measurement had previously been applied, with the simplifying approximation of axial symmetry, to long-standoff PAW and to GTAW. It has now been discovered that the continuum radiation, which required a minor correction in those analyses, is actually stronger than the spectral line radiation from a short-standoff PAW plasma. Infrared lines, free of such interference, have therefore been identified and will be used for systematic correlation of temperature distributions with eight welding parameters and with weld quality.

2.0 BACKGROUND

2.1 Viewpoint

The reason for undertaking this project is the conviction that understanding of the physical phenomena underlying the plasma-arc welding (PAW) process will help reduce the time and total development and production costs required to achieve the process's fullest fabrication capability, as measured by penetration, quality and reliability. Modern ships and other structural systems require increasingly complex fabrication of advanced materials to stringent quality standards, but development of the needed welding procedures depends almost entirely upon the costly, intuitive, trial-and-error methods traditional to welding engineers. Process development costs could be reduced significantly by measurement of key physical observables, mathematical modeling of critical elements of the welding process, and implementation of the resultant teachings. Reasons for selection of PAW for such a fundamental investigation include: (a) its superiority to gas tungsten-arc welding (GTAW) in energy concentration and in tolerance of variations in joint fitup; (b) the fact that PAW had recently been used to weld inch-thick Ti-6Al-4V with a single penetration pass,[1] a penetration twice that believed possible by the manufacturer of the welding equipment; (c) the consequent potential value of PAW for fabrication of hydrofoils and surface effect ships, and (d) the fact that, except for a contribution to item (b) on this list, the development of PAW--like that of any other welding process in common use--has been wholly empirical and observational, not analytical. Even the best phenomenological discussion of factors asserted to limit process performance includes no validating calculations or quantitative measurements.[2] The causal

relationship given between torch design and weldment properties was pure conjecture. There was no predictive capability to guide torch design and parameter optimization, to set goals for attainable process performance, nor to extrapolate test results from one alloy to another; indeed, not even to other heats of the same alloy.

2.2 Importance of Temperature Distributions

The primary function of a welding device is to heat the base metal and any filler material to the melting point. (It must also control the pressure exerted on the puddle of molten material in order to regulate its motion, and thus to avoid defects of many kinds, and to enhance penetration in the keyhole mode of welding.) To eliminate all distortion, residual stresses and degradation of the heat-affected zone (HAZ), this should be done uniformly along the surfaces to be joined, without heating any metal but that melted. Unfortunately, this Utopian prescription not only requires the line-source of heat, (a source of finite power distributed over an infinitesimal area), which is found only in heat conduction theory, but requires one which moves with infinite travel speed! In the world of physical reality, one cannot always use the highest available power density and travel speed because of imperfect joint preparation and fitup, and because of the need to control puddle circulation. But it is certainly desirable to be able to control power density (as PAW torch designers say, without proof, that they do) and to determine, by as direct a measurement as practical, the power density actually produced by a PAW torch. This governed the decision to begin the PAW research with time-resolved measurement of plasma temperature as a function of position in the standoff region, between the torch orifice and the plane of the base-metal

top surface, during downhand keyhole-mode welding of titanium.

2.3 Difficulties of Earlier Work

Attempts have been made for some 20 years to understand welding processes by spectroscopic measurement of plasma temperature distributions.[3] Harry Olsen's pioneering work was a landmark in argon spectroscopy, but as welding research it was fatally handicapped by the slow experimental and analytical techniques available before now. To achieve reasonable stability during a complete scan of the arc, it was necessary to work with a stationary arc burning between a fixed tungsten cathode and a fixed, water-cooled, unmelting, copper anode. Interaction of anode and cathode regions required the arc to be much longer than is actually used in GTAW. To be able to interpret his data, he had to work with highly purified argon and avoid any trace of metal vapor. When he managed to introduce the slight degree of realism of admitting that welding arcs are not axially symmetric, and developed a method for studying an asymmetric plasma,[4-6] he had to perfect an utterly unrealistic electrode geometry which kept the arc stable for the eight hours he spent measuring it for each set of operating conditions.[5] Analysis of his data was comparably laborious.

Olsen's original method (still in common use among plasma spectroscopists) was to focus an image of the arc onto the input slit of a spectrograph. The narrow slit width spanned only a thin section of the image, normal to the axis of symmetry. The slit height was no less than the detectable width of the image. Each spectrogram thus recorded spectral lines whose density varied along their length. This was related to the variation in intensity of the light projected from the arc at various points across the given thin section.

On the assumption that the arc was circularly symmetric, Abel inversion then gave emissivity of the spectral lines as a function of radial distance from the axis of symmetry. Several methods for performing Abel inversion are given in a standard treatise on plasma diagnostics,[7] together with difficulties associated with each of them.

For the asymmetric case, Olsen determined the intensities $g(x,\xi)$ as before for each image-position x, but also for images projected on many different vertical planes each of whose normals made some angle ξ with a reference plane. He then used the fact that each spectral emissivity $f(r,\theta)$ can be represented exactly by a doubly-infinite series of known basis functions with unknown coefficients, such as

$$f(r,\theta) = (\alpha/\pi)^2 \sum_{k=0}^{\infty} \sum_{m=0}^{\infty} \varepsilon_m (-1)^k \left[k!/(m+2k)!\right] \left[B^m_{m+2k}(\alpha)\cos(m\theta) + D^m_{m+2k}(\alpha)\sin(m\theta)\right] \cdot$$

$$\cdot (\alpha r)^m L^m_k\left[(\alpha r)^2\right] \exp\left[-(\alpha r)^2\right] \quad . \qquad (1)$$

(Here ε_m is 1/2 for m = 0, and equals 1 otherwise. The $L^m_k(u)$ are associated Laguerre polynomials of degree k in the argument u.) It was next assumed that f could be approximated adequately by truncating the series in equation (1) at some finite values k = K, m = M. This basis-function approach implies that the intensities g also have a series representation, involving the same coefficients as the series for f, since f and g are related by the Abel integral equation

$$g(x,\xi) = \int_{-\infty}^{\infty} dy f(r,\theta) \quad , \qquad (2)$$

where $x = r\cos(\theta-\xi)$ and $y = r\sin(\theta-\xi)$. By use of the orthogonality conditions for the known functions appearing in the series representation for g, it was shown[6] that Eqs. (1) and (2) mean that the coefficients are given explicitly by

$$B^m_{m+2k}(\alpha) = \int_{-\pi}^{\pi} d\xi \cos(m\xi) \int_{-\infty}^{\infty} dx\, g(x,\xi) H_{m+2k}(\alpha x) \quad , \tag{3}$$

$$D^m_{m+2k}(\alpha) = \int_{-\pi}^{\pi} d\xi \sin(m\xi) \int_{-\infty}^{\infty} dx\, g(x,\xi) H_{m+2k}(\alpha x) \quad . \tag{4}$$

where $H_n(u)$ is the Hermite polynomial of degree n in u. These equations can only be used if enough data is taken to perform the indicated integrations numerically. This was done (first with simulated data) with the series truncated at $M = K = 5$. In addition to the scale factor alpha, 66 coefficients were found for calculation of emissitivity in each horizontal section. Each coefficient-set calculation employed 5957 values of intensity g, taken at 161 points x for each of 37 orientation angles.

2.4 New Factors Permit Simplification

Experimental and analytical techniques have recently been created which permit acquisition, during actual welding and at snapshot speed, of data with the same information content as Olsen could gather from his stabilized arc in a full day. These techniques vastly reduce both the experimental and the analytical labor required, and thus make systematic study of temperature distributions in a realistically unsymmetric welding plasma truly practical. Such an advance was possible because four factors, none of which was available to Olsen, were brought together for the first time.

2.4.1 Interference Filters

The first factor is the use and commercial availability of image-quality thin film interference filters with bandwidth narrow enough and shape factor (ratio of width at 0.1% of maximum transmission to width at half maximum transmission) good enough to allow a plasma to be photographed by radiation from only a single spectral line. The full height, not a thin section, of the plasma is recorded. By use of beam splitters and multiple mirrors and filters, the arc radiation can be recorded for as many wavelengths and view directions as are actually required.

2.4.2 Two Analytic Improvements

Analysis was simplified in two stages, and the improved analysis permitted further reduction of the experimental effort by reducing dramatically the number of views of the plasma which need to be recorded.

First, the method of best accessible estimation was created for solution of "improperly posed" problems, a category which includes the Abel integral equation.[8,9] Practical application to plasma diagnostics was first made for a symmetric arc.[10] With computation stabilized by this method, much less redundant data is needed to determine the distribution of two spectral emissivities as functions of position. The temperature distribution can then be calculated from the local ratio of emissivities according to the two-line method,[7] which is insensitive to contamination of the plasma by metal vapor and other impurities, which are always present during welding.[11] The second improvement concerned the asymmetric case. One can show that no finite number of projections (photographs, spectrograms, etc., recorded for different view directions)

permits exact reconstruction of the desired distribution. However, a very simple expression has been derived[12] which gives the minimum number of projections required to give any desired degree of angular resolution in the reconstruction, and relates the degree of radial complexity of the reconstruction to the number of data points which can be resolved in each section of a projection. For temperature distributions of the limited azimuthal complexity we anticipate, two projections are adequate, not the 37 prescribed in Ref. 4. Best accessible estimation was used again to stabilize the calculation and take proper account, statistically, of the limited precision of measurements and calculations. Applied to the same simulated data as used in Ref. 4, the new method gave comparable errors with 160 data points instead of 5957.

Since we avoid taking enough data to perform the numerical integrations, we do not find the coefficients for Eq. (1) from Eqs. (3) and (4). A different normalization and nomenclature for the coefficients is therefore convenient. We re-write Eq. (1) as

$$f(r,\theta) = \left(\alpha/\pi^{1/2}\right)\exp\left[-(\alpha r)^2\right]\sum_{m=0}^{\infty}\sum_{k=0}^{\infty}(-4)^k k!\,(2\alpha r)^m L_k^m\left[(\alpha r)^2\right]\cdot$$

$$\cdot\left[C(m,k,\alpha)\cos(m\theta) + A(m,k,\alpha)\sin(m\theta)\right] \quad . \qquad (5)$$

If that expression is substituted into Eq. (2) and the integration performed analytically, one finds by the same methods used in Appendix A of Ref. 6 that

$$g(x,\xi) = \exp\left[-(\alpha x)^2\right]\sum_{m=0}^{\infty}\sum_{k=0}^{\infty} H_{m+2k}(\alpha x)\left[C(m,k,\alpha)\cos(m\xi) + A(m,k,\alpha)\sin(m\xi)\right] \quad . \tag{6}$$

Our technique is to regard Eq. (6), evaluated at each point x on each view defined by orientation angle ξ for which g is measured, (for a thin horizontal section through the plasma at some distance z below the torch orifice, as photographed by radiation from one spectral line), as a set of simultaneous linear equations for the coefficients C and A. (Determination of alpha is covered later in Section 3, "Progress.") The simultaneous equations could in principle be solved by matrix inversion or equivalent algebraic methods. However, the matrix involved is usually ill-conditioned, which means that small errors in measurement (or simply the roundoff error which is unavoidable in computer analysis) would cause gross errors in the calculated values of the C's and A's. That is why they are found instead by best accessible estimation.

If density can be found at pre-selected positions, symmetry properties of the known functions in Eq. (6) can be used to reduce the number of computational steps by a factor of 16.[13] (There is an error in the rule suggested in Ref. 13 for choosing values for ξ. Actually, one should try to avoid values which are rational fractions of π or of one another--except, in the latter case, where the rational fraction is -1.) Once the C's, A's and α have been found for each spectral line the temperature at the time the shapshot was taken can be calculated at any point by the two-line method[4,10] as

$$T(r,\theta,z) = \frac{E_1 - E_2}{k \log[A_1 g_1 \lambda_2 f_2(r,\theta)/A_2 g_2 \lambda_1 f_1(r,\theta)]} \qquad (7)$$

where k is the Boltzmann constant, the subscripts i = 1 & 2 refer to the two spectral lines employed to take the photographs, g_i here is the degeneracy and E_i the energy of the excited state which emits the light of wavelength λ_i, A_i is the Einstein transition coefficient for spontaneous emission of the line, and $f_i(r,\theta)$ is, of course, given by the truncated version of Eq. (5), for which the coefficients were calculated as just described. The coordinate z determines the section of each image within which intensities are found. The quantum mechanical quantities are all known theoretically or experimentally. The partition function, which Olsen had to calculate for his pure argon, is one of the factors which cancels out of the temperature-determining equation when the two spectral lines are chosen from the same species--say both for neutral argon, or both for singly-ionized argon.

2.4.3 Minicomputer Utilization

Despite the improved analysis and the experimental improvements, we will still be measuring film density as a function of position at more than a thousand points in the set of four images produced in each test. We can make up to six tests per weld, and need to run hundreds of welds. Clearly, computer automation of data acquisition (see Section 3, below) must be made as complete as practical. Availability of a minicomputer which can be configured for and dedicated to this on-line function is another major advantage over earlier investigators.

2.4.4 Display Languages

Interpretation of the temperature distributions in terms of welding parameters and their relationship to properties of the weld and HAZ almost demands that the temperature data be displayed graphically, and in multiple views. Computer-controlled graphical output has been available for years, but only recently have computer languages been introduced specifically for producing contour maps, isometric projections and other displays of numerical or analytic information. Use of three such languages, each superior to the others for certain applications, constitutes the final of our four advantages over previous welding-plasma spectroscopists.

3.0 ACCOMPLISHMENTS

The theory we employ has been described above in Section 2, "Background." It requires a plasma image, from which projected intensity of radiation can be calculated, in two directions through the plasma, at two selected spectral wavelengths of one neutral or ionized species in the plasma. The experimental apparatus required has been designed, fabricated, and aligned to the meticulous standards necessary. All the calibration procedures required have been defined and executed. A minicomputer has been configured and programmed for partially automated data acquisition from each set of four images scanned by a microdensitometer. The minicomputer scales the data, sorts and refiles it as required, and solves for the parameters which determine temperature. These are transmitted to the larger computer which generates graphical displays of the temperature distribution. Only sample displays were generated from experimental data in the report period, but each step in the experimental and analytical procedure has been proof-tested. It has been discovered that, at the wavelengths used for the initial tests, there is far more continuum radiation from a PAW plasma of given current and standoff than from a GTAW plasma of the same current and standoff. The continuum is also substantially stronger, relative to the spectral line intensities, than when chord-averaged temperature was measured for PAW on thicker specimens of the same titanium alloy, i.e., when twice the present standoff was used. As a result, it was judged unprofitable to attempt extensive quantitative analysis, interpretation and display of the initial data. Spectral lines have been selected for future use which avoid the need to correct the observed data for superimposed continuum radiation.

The following subsections describe these results in more detail.

3.1 Experimental Apparatus

The photographic images in two view directions and two monochromatic wavelengths are obtained in the apparatus shown schematically in Fig. 1. The inert atmosphere box (I) contains a Linde PT-8 plasma arc welding torch and a translation carriage mounted on two rods which moves a water-cooled grooved copper backing bar carrying the weld specimen plate past the stationary torch position. A screw cutting lathe coupled to a draw bar attached to the specimen carriage provides the translation speeds. View ports at appropriate positions in the box wall allow the plasma radiations to enter the two-directional optical system (II) and the monochromator (IV). The lens (L) forms a near-unity magnification image of each view path at plane (P). The purpose of this system is to compress the large angle between the view directions ($\sim 87°$) into a small one of about 3° which can be handled in the two-wavelength camera optics (III). The first objective lens of the camera system (III) forms an image of plane P (and its plasma images) in the plane of the beam splitter which divides the resultant images into two paths. Each of these paths contains an appropriate monochromatic narrow-bandpass filter (F_1) and (F_2) in front of the camera lens which images the beam-splitter at the film plane of the cameras.

The bandpass filters F_1 and F_2 are really two-cavity interference filters of image quality. The companion filter to F_1 and F_2 is a broad bandpass filter spanning a little more than the wavelength interval between F_1 and F_2 and is mounted in front of the first objective of II. In the initial experiments the filters were centered on ionized argon lines at 488.0 nm (F_1) and

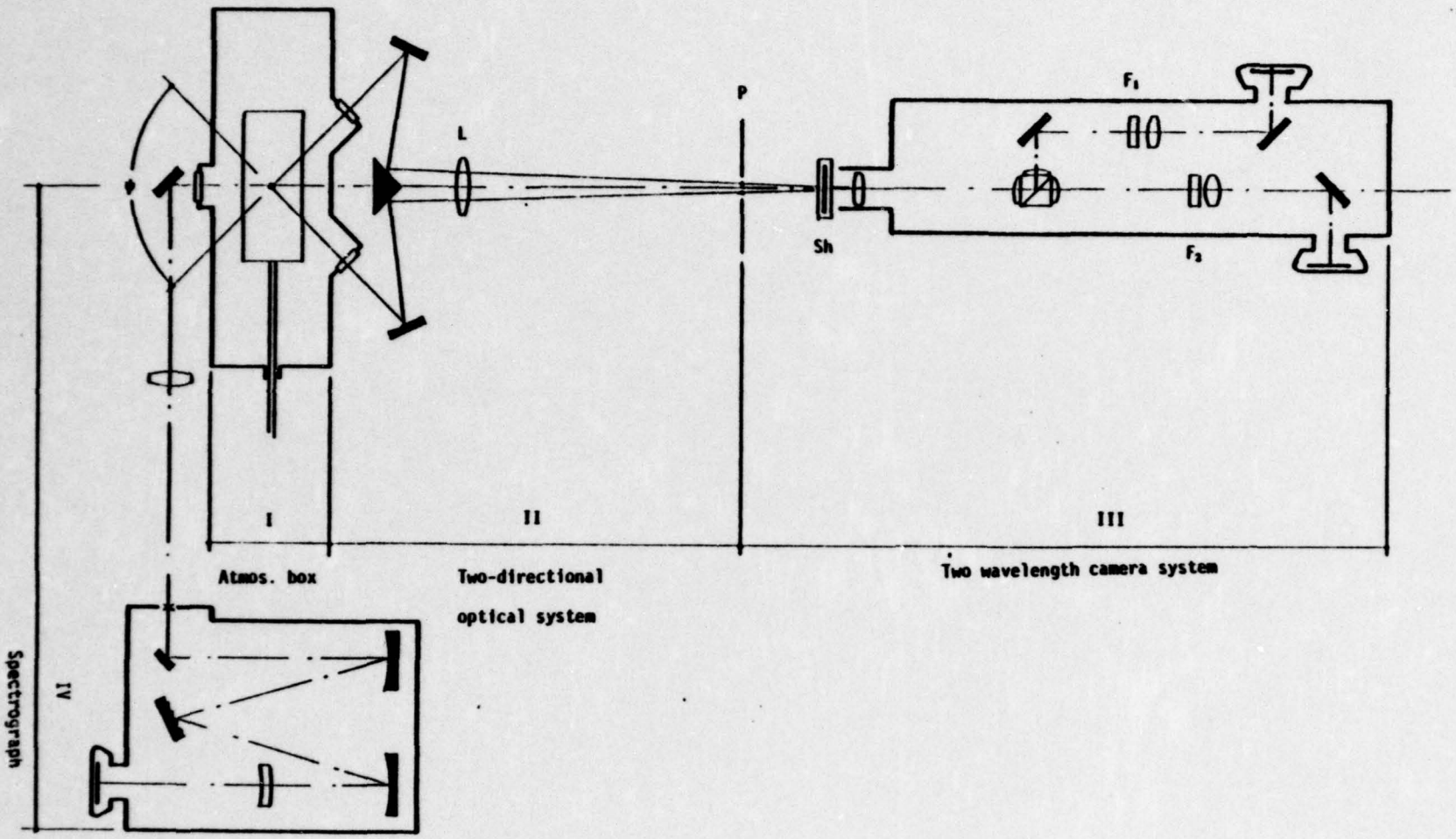

Fig. 1 Schematic diagram of the experimental apparatus

480.6 nm (F_2) with 0.3 nm FWHP. These were the lines we used for previous welding-plasma temperature measurements.[1,10]

A Compur type shutter (Sh) in front of the first objective lens of the camera systems controls the duration of the simultaneous exposures at the two film planes. In order to estimate the relative intensities of the two spectral lines above the background continuum, a third path is used which is normal to the travel of the specimen. The plasma image is focused at the input slit of a Heath-Schlumberger Model EU 700/E Scanning Monochromator--modified for spectrography. A 35 mm camera records the torch spectrum from about 470 nm to 510 nm. Exakta camera bodies are used to hold and advance 35 mm film for all exposures. The film strips are developed simultaneously completing the data recording process.

A PhotoMetrics, Inc., EDP Scanning Microscope provides densitometric analysis of the various images and calibrations. As the instrument scans the film sample on the optical stage a simultaneous record is processed on a facsimile stage at one of several selectable enlargements. The circuitry within the instrument quantizes the voltage, representing density value, and produces isodensity contours on the facsimile enlargement.

A Data General Corp. Nova 2/10 minicomputer with high-speed tape and triple cassette drives, analog data system, digital input-output, and communication interface is used to analyze and store large files of data taken from the photographic images. It also handles the analytic programs to reduce the position vs. density information to the relatively small number of parameters needed for Eq. (5), to generate position vs. temperatures maps of the plasma region. It communicates the parameters to a larger computer for

further manipulation, interpolation, and graphic display of the temperature distributions.

Figure 2 shows representative microdensitometer scans of typical image data. The upper figure shows the isodensity contour representation of a plasma image while the lower figure is a linear microdensitometer scan of the spectrogram used to evaluate the continuum radiation contained in the exposures.

3.2 Calibration and Data Reduction Procedures

To determine temperature as a function of position, $T(r,\theta,z)$, from the photographic images requires the determination of several reduction factors which are not apparent from the description of the experimental apparatus. These parameters include the angle between the view directions and an orientation angle relating the view direction(s) to the weld direction, freeing the image densities from the effects of magnification, transmission losses and plasma continuum radiation and finally conversion of the densities to corresponding intensities.

3.2.1 The Determination of Magnification and View Angle

The angle between the two views and the magnification of the images on the film were obtained simultaneously through a two-step process.

A 4 mm × 6 mm reticle was placed parallel to the weld direction in the position normally occupied by the plasma arc in the atmosphere box and illuminated so that its image was visible in the focal plane (P) of Fig. 1. The photographic images were measured in the vertical plane and compared with the original to determine the magnification of

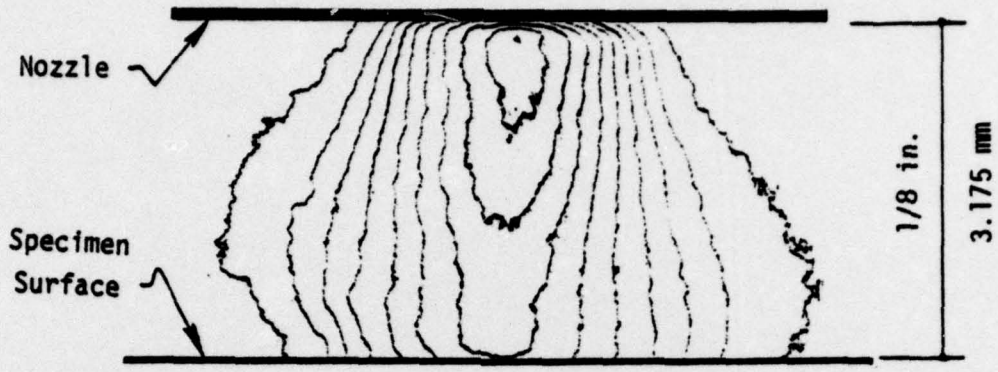

a. Isodensity contours of a plasma image for one direction and one wavelength

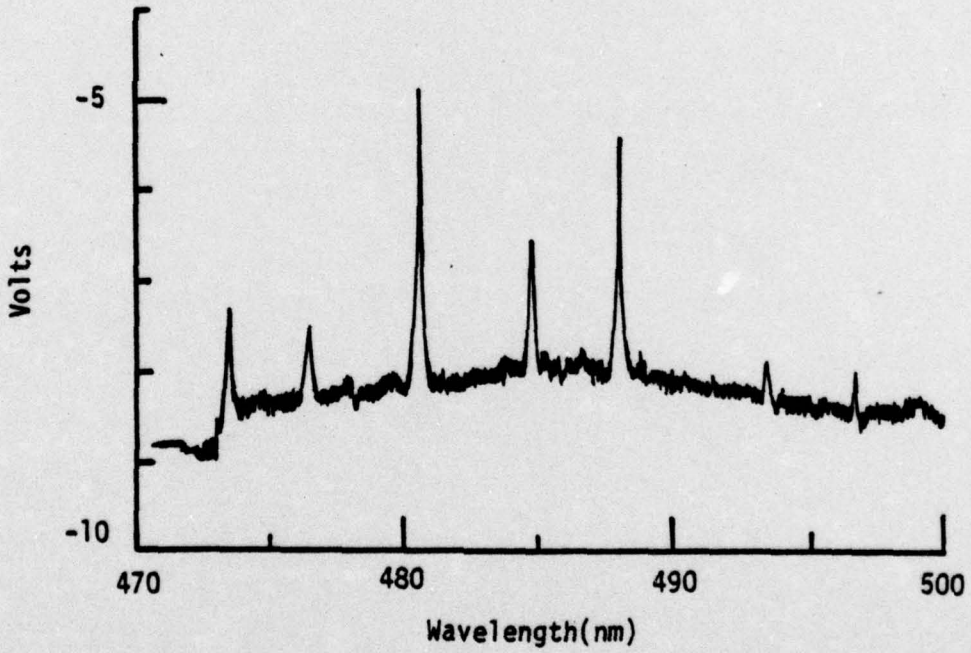

b. Linear slit scan of a spectrogram used to evaluate the continuum radiation contained in the plasma image exposures

Fig. 2 Representative microdensitometer scans of typical image data

the images to that point of the optical path. The horizontal sections of the two images were then measured to obtain the cosine of the angle of the view from the optical axis of the system. The total angle ψ between the two views determined in this manner was found to be 86.97° and the angle between the normal to the weld direction and the left-hand view direction was 43.00°. A second determination of these angles at a later time indicated an uncertainty of about 0.1°.

In order to determine final magnification at the film plane the test target was placed at the image plane (P) of the previous step and illuminated. Photographs were taken of both the 480.6 nm and the 480.0 nm images and again measured and compared with the original to determine the magnification. The overall magnification (arc to final image plane) for the 488.0 path was M_{80} = 1.4700 while that for the 480.6 path gave M_{06} = 1.5727.

3.2.2 Determination of the Optical System Transmission

The throughput of light from the source to the images recorded on the photographic film (Fig. 1) is subject to a variety of losses (absorption, reflection, scattering, etc.) which are spectrally and positionally dependent. Our requirement for transmission calibration is a source whose log intensity ratio is known at the two wavelengths so that it can be compared to the recorded image densities. A 100W zirconium lamp was calibrated for this purpose and found to have an effective source temperature of 2621±49°K. Using this temperature, the theoretical intensity ratio at the required filter wavelengths is

$$\frac{I_{80}}{I_{06}} = \frac{I_{488.0}}{I_{480.6}} = 1.1017 \quad . \tag{8a}$$

The zirconium lamp was then placed at the source position (Fig. 1) and images of the lamp recorded at the film planes. The maximum density of each image was found from the microdensitometer scans of the images. Assuming the results of the film calibration techniques to be described in a later section, the measured intensity ratio was $I_{80}/I_{06} = 1.2448$. The transmission factor is obtained from the above-found intensity ratios and the previously-determined magnifications,

$$\frac{T_{80}}{T_{06}} = \frac{(I_{80}/I_{06})_{MEAS.}}{(I_{80}/I_{06})_{THEOR.}} \cdot \frac{(M_{80} + 1)^2}{(M_{06} + 1)^2} \tag{8b}$$

$$= \frac{1.2448}{1.1017} \cdot \frac{(1.4700 + 1)^2}{(1.5727 + 1)^2} = 1.0415 \quad .$$

Hence, the 488.0 path has 4.15% higher transmission than the 480.6 path.

3.2.3 The Determination of Intensity

The microdensitometer calibration consists of determining the trip voltages representing isodensity contours (contour numbers) on the facsimile scan pictures and relating the corresponding photomultiplier amplifier output voltage to a standard grey scale. The film density comparison standard was a calibrated Stouffer 30-step density scale.

The microdensitometer was also used to determine the characteristic exposure curve (Density vs log I) for Plus X film exposed for 1/25 sec.

and developed in D-19 for 5 min. at 20°C. The exposure data at 480.6 nm and 488.0 nm were found to be within a standard deviation of each other so that the average of the two was used to describe both.

Figure 3 combines the results of the microdensitometer calibration and the Plus X exposure curve. Curve C relates contour number (top scale) to voltage (left scale). Curve D relates voltage (left scale) to density (bottom scale). And Curve E relates density (bottom scale) to log intensity (right scale). Thus, a contour number or density can be appropriately converted to log I and thus to intensity.

All factors are now at hand to correct the recorded plasma image densities to theoretically ideal plasma intensities as required by the computer code to determine the temperature distribution in the plasma. As an example, an x,y position intersecting a contour line (Fig. 2) can be converted to an x,y position in the plasma coordinate space through reduction by the magnification. The contour level (number) representing a density is converted to an intensity, I, which is the sum of the argon ion line radiation plus the continuum radiation at that wavelength. The fraction of the line radiation, p, with respect to the total can be found from the spectrogram scan (Fig. 2) after conversion of voltage levels to intensity as $p = (I_{pk} - I_{cont})/I_{pk}$.

Combining all factors to express the theoretically-ideal intensities at the two wavelengths we have

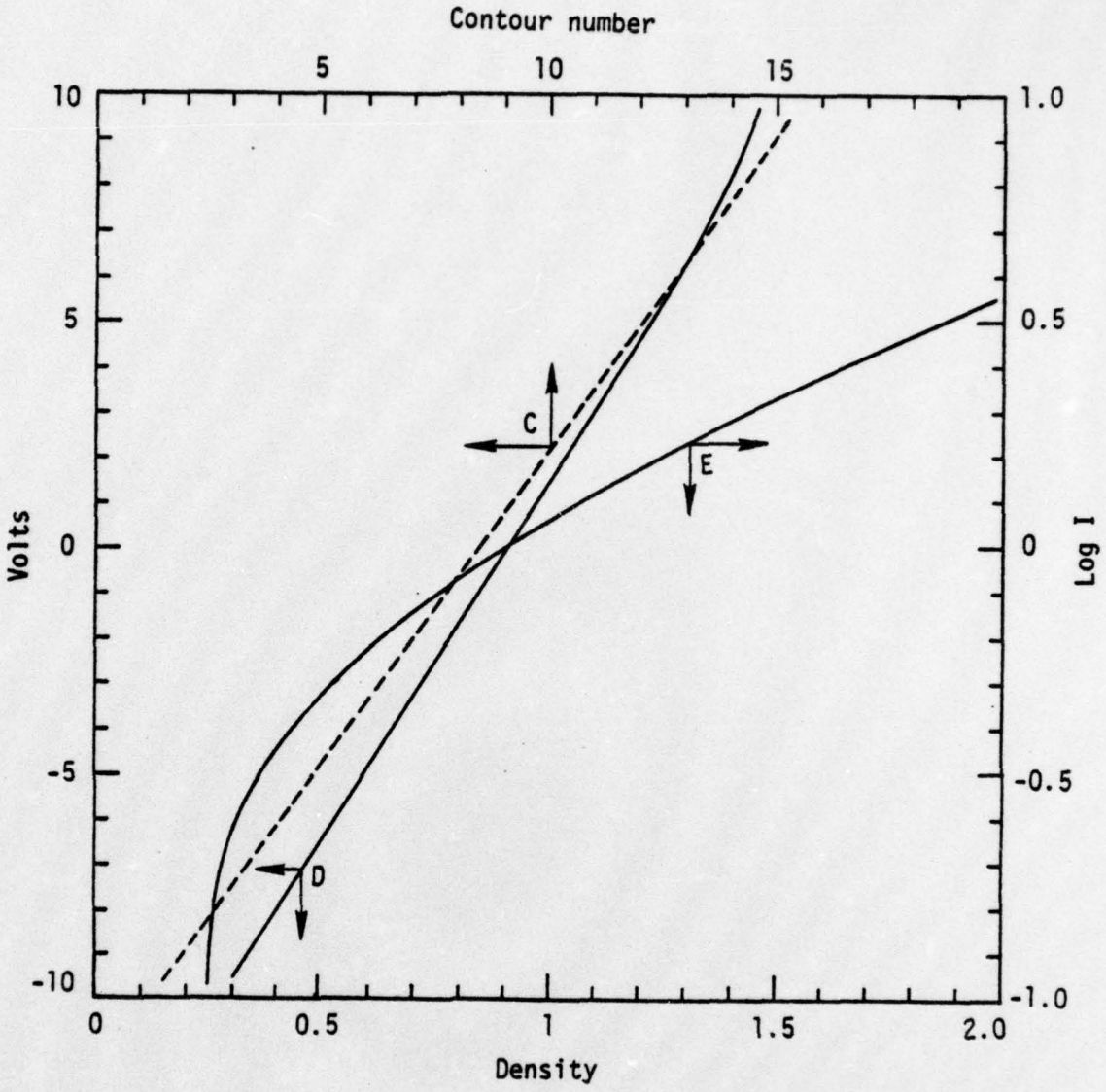

Fig. 3 Microdensitometer and Plus X film calibration curves

Curve C relates contour number to voltage
Curve D relates voltage to film density
Curve E relates film density to log intensity of exposure source

$$I_{06}\Big|_{THEOR.} = I_{06}\Big|_{MEAS.} \times \frac{1}{T_{06}} \times (M_{06} + 1)^2 \times p_{06}$$

$$I_{80}\Big|_{THEOR.} = I_{80}\Big|_{MEAS.} \times \frac{1}{T_{80}} \times (M_{80} + 1)^2 \times p_{80} \qquad (9)$$

3.3 Data Analysis

3.3.1 Data Input Procedure

After obtaining the contour images from the microdensitometer, each contour map in turn is placed on a Hewlett-Packard X-Y recorder whose pen has been replaced by a light pipe sight with a fine cross-hair reticle. Two channels of the A/D conversion system of the Nova 2/10 parallel the recorder inputs. The procedure is to orient the contour map to the recorder and make horizontal scans at selected Y intervals. Then, for each Y value, the X voltage is adjusted to place the cross-hairs on successive contours. Typing of the contour numbers on the teletype triggers A/D conversion of the X voltage, which is recorded as a binary integer together with the corresponding contour number.

The following data then have to be stored in a cassette file to permit further processing: for each image, an image label and the number of scans made of that image; for each scan, the ordinal number of the scan, the output of the Y-A/D converter, the number of contour lines which were cut, and all the data pairs (contour number and the output of the X-A/D converter) which were generated.

A table look-up is used to go from contour number to logarithm of intensity (for estimating the scale factor α) or to intensity. After

the conversions have taken place the image identifier, intensity and position values, estimated α, and the scan number and data-pair count are filed for the four images.

3.3.2 Scale Factor Estimation and Data Sorting

Three methods for estimating α from the data have been explored. Two, which involved nonlinear rather than linear least-squares fitting techniques, were discarded not because of complexity but because of instability. The simplest method of all proved most reliable. It assumes that the first term in the series expansion for $g(x,\xi)$ is the dominant term, and makes the crude approximation

$$g(x,\xi) = C(0,0,\alpha)\exp\left[-(\alpha x)^2\right] \tag{10}$$

for each ξ, in the notation used in Section 2. Note that for any section z, α is the same for both images formed by a single spectral line, but definitely not for those formed by different lines. On taking the natural logarithm of both sides in Eq. (10), one has a linear equation in x^2 of the form

$$\ell n\left(g(x,\xi)\right) = a + bx^2 \tag{11}$$

where $b = -\alpha^2$. Hence, when a linear least-squares fit is made of logarithm of intensity of x^2, using data for the scan in both views with one spectral line, α is the square root of the negative of the slope. The standard formula for the linear least-squares slope is used to estimate α as

$$\alpha = \left\{ \frac{(\Sigma x^2)(\Sigma \ell ng) - (n_1 + n_2)\Sigma x \ell ng}{(n_1 + n_2)\Sigma x^4 - (\Sigma x^2)^2} \right\}^{1/2} \qquad (12)$$

where n_1 data pairs were recorded for one view, n_2 for the other, and the sums extend over all $n_1 + n_2$ data pairs for each wavelength and scan number. (A warning is output in the unlikely event that a positive slope is computed.) The estimated scale factor is further refined in the course of solving Eq. (6) for the coefficients needed in Eq. (5), the basis-function representation of the local emissivities of the two spectral lines.

3.3.3 Evaluation of Coefficients

In accord with the theory of reconstruction from a few imperfect projections,[12] use of only two view angles permits estimation of the coefficients of terms whose angular dependence is given by a constant term and by the sine, cosine, and sine of twice the angle. The complexity of radial dependence is governed by the number of independent measurements which can be made on each projection. In the present case it was judged that realistic physical variations in emissivity could be represented by fourth degree polynomials, for which enough data was at hand to give satisfactory redundancy. For each slice z and for each wavelength, Eq. (6) was solved (simultaneously for all x, on the two projection planes, for which intensity g was measured) for the nine unknowns: $C(0,0,\alpha)$, $C(1,0,\alpha)$, $C(0,1,\alpha)$, $C(1,1,\alpha)$, $C(0,2,\alpha)$, $A(1,0,\alpha)$, $A(2,0,\alpha)$, $A(1,1,\alpha)$, and $A(2,1,\alpha)$.

As previously indicated, solution of the simultaneous equations required the (reduced) method of best accessible estimation (BAE)[8,9] since the system of equations is too ill-conditioned for direct solution. The background and measurement-error processes were assumed to be independent white-noise processes of equal variance, a condition which was sought by using the proper aperture in the scanning microdensitometer. (Too small an aperture gives rough contours as the densitometer tries to resolve individual film grain-clumps, while too large an aperture smooths away real variations in recorded intensity.) In this case the finite-iteration formula of Eq. (4.9) in Ref. 9 simplifies to

$$u_n = (A^*A + I)^{-1}(A^*g + u_{n-1}) \tag{13}$$

for the n-th estimate of the solution to

$$Au = g \tag{14}$$

with u_o defined as 0. A sensitive test for the maximum order of iteration to be used, because of the accumulation of numerical error, is given in Ref. 9. In Eq. (13), the unit matrix is represented by I and A* is the adjoint to the matrix A of (14), the symbolic form of (6) in which u is the column vector of the nine unknown coefficients. The inverse shown in (13) is not computed explicitly; in the interest of computational efficiency, the equivalent set of simultaneous equations is solved by back-substitution with full scaling and pivoting. The assumption of

equal variance for the white-noise processes was tested empirically and found valid. (For unequal variances, their ratio multiplies I and u_{n-1} in (13). See Ref. 9 for details.)

Since the successive estimates generated by BAE would (in the absence of numerical round-off error) converge to the minimum-residue estimate of minimum length (in the appropriate norms defined in Ref. 9), which is just the familiar least-squares solution of the overdetermined linear system (14) for the simple noise types assumed here, it is natural to use the residue r_N as a measure of how well the final iteration u_N fits the experimental data. The residue is given by

$$r_N^2 = (g - Au_n)^*(g - Au_n) \tag{15}$$

and is a measure of how much of the observed data vector g is unaccounted for by the n-th estimate. Our computer program therefore reports the final value of r_N as a fraction of the norm of the data, that is,

$$r_N/\sqrt{(g^*g)} \quad . \tag{16}$$

However, before this is done, the BAE solution u_N, and the corresponding residue r_N, are stored while a different value of the scale factor α is used in Eq. (14)--the symbolic representation of (6)--and again the BAE solution and residue are found. A systematic search is performed for the value of the scale factor which gives minimum r_N, to any desired precision. This is a time-consuming process, but unconditionally stable,

in contrast to the nonlinear methods tried for optimization of α as described in the preceding subsection. This would seem to indicate that Eq. (6) with the nine coefficients indicated fits the data much better than the single-term approximation, Eq. (10), and suggests a future attempt to use Newton's method to find that scale factor for which r_N has its global minimum. The quadratic convergence of such a method, now we are reasonably certain it will be stable, should reduce minicomputer time requirements by a factor of six or seven, to about three minutes per case, to judge by the several dozen cases investigated to date. The use of basis functions means that the derivatives needed for Newton's method can even be found analytically; numerical approximation to them is not needed.

Figure 4 shows a typical data set, intensity versus position for the two view directions or projections, and the values calculated for the same x and projection angles when the best estimate u_N is used for the indicated nine coefficients in Eq. (6). With the optimum value of the scale factor, r_N was less than 3% of the rms data.

3.3.4 Temperature Distributions

Having found u_N (the set of nine coefficients) and the corresponding scale factor which minimizes the residue r_N, the emissivity $f(r,\theta)$ can be found from Eq. (5) for any point in the plane z for which the intensities were measured from the photographic images. Two such solutions, one for each wavelength, or 20 numbers in all, then permit evaluation of Eq. (7) to give $T(r,\theta,z)$ anywhere in the given z-plane. If isotherms are desired, the use of basis functions again means that all

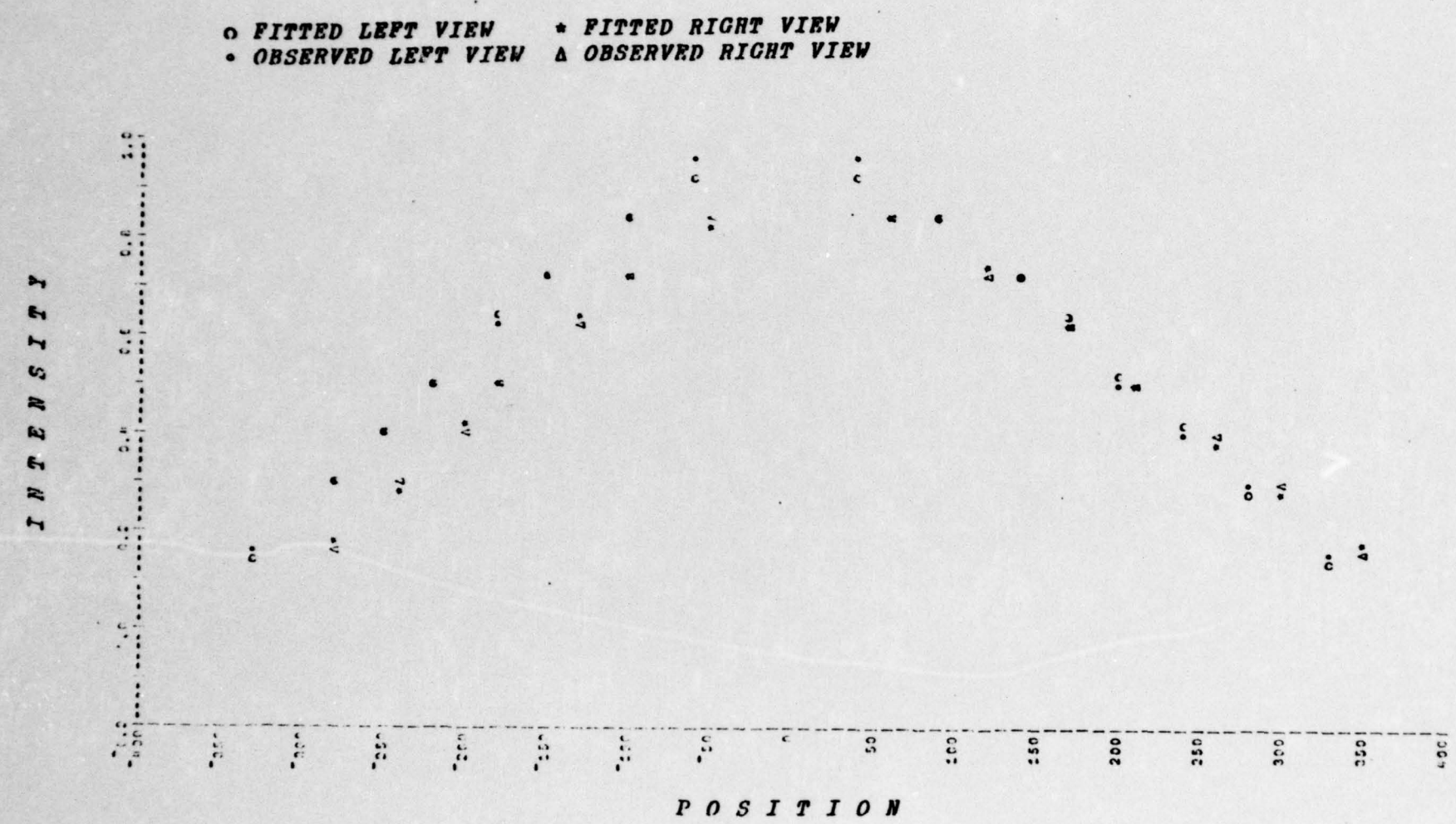

Fig. 4 Observed and fitted values of intensity at 480.6 nm vs position for Exp. 135 (80 amps). Section taken near the nozzle.

differentiations needed for rapid calculation of isothermal locus can be carried out analytically. Figure 5 shows comparative values of $T(r,\theta)$ for the four planes $\theta = 0°$, 45°, 90°, and 135° where 0° is the line of welding, in the direction of torch travel relative to base material. In each case, a negative value of r is to be understood as positive r in the (half-) plane $\theta + 180°$. The same data, simply cross-plotted for a few values of temperature, yields the isotherm map of Fig. 6. A 1 mm scale is included to indicate the small extent to which the maximum temperature, and the plane of quasi-symmetry of the isotherms, is offset from the line of welding, and the distance the maximum temperature trails the torch axis. The temperature gradient is seen to be asymmetric fore and aft, as expected.

While the exhibited temperature distribution is of plausible shape and magnitude, it is not meaningful to compute and interpret comparative temperature distributions as functions of welding parameters, such as current, at this time. This is true even though photographic and spectrographic data were recorded, both for a steel alloy and for 6-4 titanium, at currents which just achieved full penetration in square butt joints, and at currents slightly above and slightly below full-penetration values. (The preceding statement describes only a few days work, including film processing.) However, as it happens, the experiments in question had to be conducted and analyzed, insofar as possible, at a time when the microdensitometer had failed and was being totally rebuilt. The calibration and data reduction procedures described in Subsection 3.2 above therefore could not be applied to the actual experi-

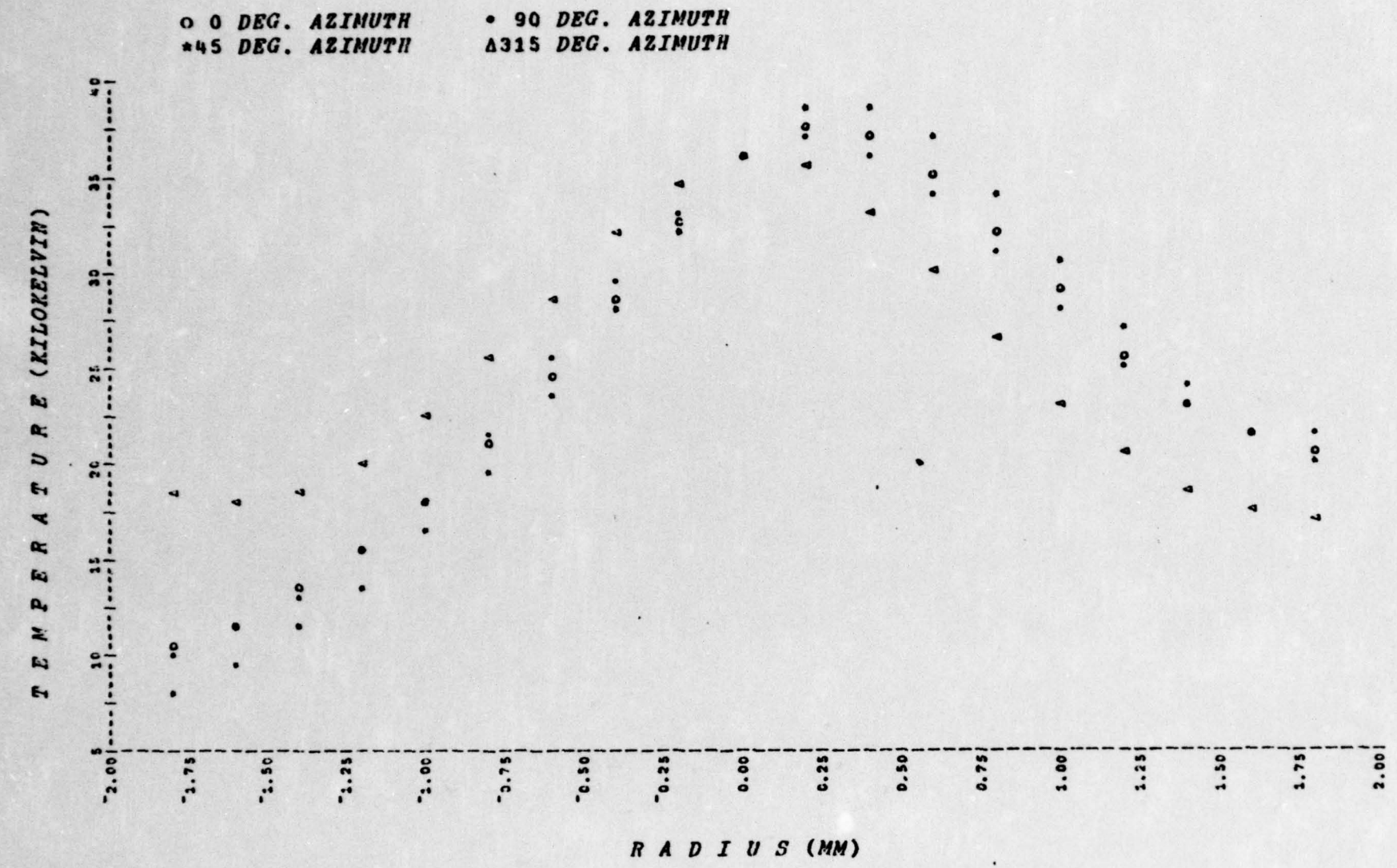

Fig. 5 Temperature vs radius at four azimuths for Exp. 135 (80 amps). Section taken midway between torch and workpiece.

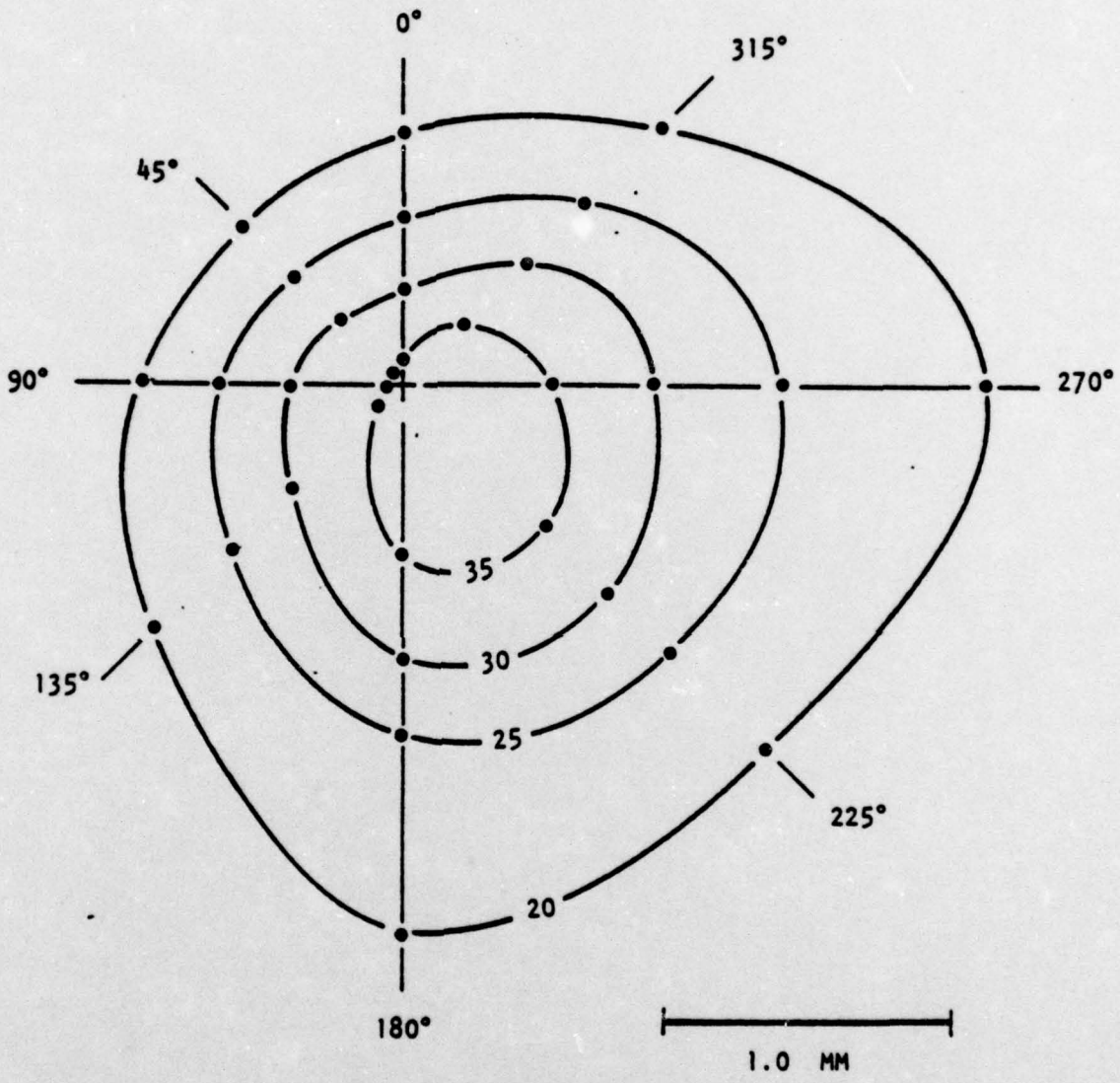

Isothermal contours (Kilokelvin) for slice 6, Exp. 135, PAW on Ti, 80 amps, 4 ipm. The isothermal levels were derived from interpolation of the temp. vs radius profiles computed at four azimuth angles.

Fig. 6 Representative isotherms determined from sections in Fig. 5.

mental data before the very end of the report period. Thus it was not established that, in these tests, the continuum radiation had been too strong to be accounted for adequately by the previously-successful simple method shown in Eq. (9), until it was too late to design, set up, and utilize a modified procedure with which to repeat the welding tests.

3.3.5 The Correction for Continuum Radiation

In Eq. (9) it was assumed that, for either wavelength, 480.6 or 488.0 nm, a constant fraction, p_{06} or p_{80}, respectively, of the intensity recorded at each point in either image (i.e., either view direction as photographed at the given wavelength) was actually due to emission of the indicated spectral line. The remaining fraction ($1 - p_{06}$ or $1 - p_{80}$) of the intensity was attributed to continuum radiation falling within the narrow passband of the filter which nominally selects the desired spectral line radiation. In GTAW studies, p_{06} and p_{80} have been found to be on the order of .93, never less than .90. More importantly, since it is only the natural logarithm of the ratio of emissivities which enters into the temperature calculation in Eq. (7), the importance of the continuum correction can be estimated from the logarithm of the ratio of p_{06} to p_{80}. For GTAW, we have never seen that ratio differ from unity by more than .03, with .01 more common. When the continuum correction affects the calculated temperature by only a few percent at most, clearly a crude approximation can be made as to the spatial dependence of that correction term--such as assuming it to be a constant fraction for each wavelength in each test--without noticeable distortion of the computed temperature distributions.

In previous PAW studies, we had observed continuum radiation at 480.6 and 488.0 nm which was appreciably stronger--up to 30% of the total passed by either narrow-band filter--than the 10% maximum seen in GTAW radiation. The continuum contribution at the two different wavelengths might differ by 10% instead of 3%. This posed no great difficulty at the time, since chord-averaged, rather than spatially-resolved, temperatures were being sought. The continuum correction described above gave temperatures which seemed entirely reasonable. More important, it gave temperatures, as functions of welding parameters, in a way which served the technological purpose then at hand in an entirely satisfactory way. The results of these earlier studies were reported in the Second Interim Report, 1 April-30 June 1974, of Ref. 1, pages 6-8, Tables IV-VI, and Figures 16-22. As shown there, photographs of the PAW plasma taken by continuum radiation alone, at a line-free wavelength between 480.6 and 488.0 nm, like photographs taken at these two wavelengths, showed very similar, essentially columnar, distributions of intensity. The continuum-only intensity is perhaps slightly stronger near the workpiece. (For GTAW, it is dim everywhere, but less so in a very thin layer--tens of μm--near the workpiece.) The continuum-plus-line intensity is stronger near the torch orifice. Anticipating that the continuum correction would be somewhat more important than for GTAW when our new PAW data was used to compute spatially-resolved temperatures, an attempt was made to improve the correction procedure. Instead of being restricted to a single average fraction p_{06} and a single p_{80} for each test, while waiting for the manufacturer to return the

microdensitometer we undertook to record spectrograms from which at least the rough spatial dependence of p_{06} and p_{80} could be determined. We hoped to estimate these correction-factor fractions as functions of radius in three horizontal planes: near the torch orifice, in the mid-plane, and near the workpiece. A Dove prism, oriented to rotate any transmitted scene through 90°, could be used in combination with a well-corrected objective lens to focus radiation from a thin horizontal section of the plasma (at one of the three indicated locations) onto the vertical entrance slit of the monochromator, and three spectrograms could be recorded. It was assumed that variation of intensity along the slit height, for any given wavelength position on the spectrograph, would indicate transverse variation of the intensity of the plasma radiation. Such refinement was abandoned, however, when it was found that the optical aberration of the available monochromator was excessive for an application so remote from its designed function. It uses focusing mirrors which operate far off axis, and therefore cannot be adjusted to resolve a radiation source simultaneously as to wavelength, horizontal and vertical position, when the source is the size of our plasmas.

In any event, microdensitometry (interpreted with use of the film exposure calibration) has now established that for the small (3 mm) standoff used in our tests, the continuum radiation is actually greater than the line radiation in the passband of the filter used--values of p were found as small as 0.4 to 0.3. Unlike PAW with longer standoff, and in sharp contrast to GTAW, the continuum correction is not a small matter

to be approximated roughly in spectroscopic measurement of short-standoff PAW plasma temperature distributions.

4.0 FUTURE PLANS

The two-line method of emission spectroscopy will be used for systematic measurement of plasma temperature, during actual PAW of titanium. To circumvent any uncertainty, due to the strong continuum radiation which has been found to obscure the lines used in prior studies, a pair of lines will be used which are free from measurable continuum background. Several such line-pairs have been identified in the ArI (neutral argon) spectrum, but they lie in the near infrared. They were not used in the initial tests because it was felt that the alignment and calibration procedures, described above, were complex enough that they should be worked through first using visible radiation. Now the filter holders will be modified with kinematic mounts to allow quick substitution of infrared filters at F1 and F2 of Fig. 1 for photography after dummy (clear) filters of equivalent optical thickness have been used at F1 and F2 during alignment and focusing. The intensity-density characterization of an appropriate infrared-sensitive film will be carried out as it was for the visible-light film. Grain size and resolution can be evaluated quickly, to determine if a change in microdensitometer scanning aperture is desirable to maintain the optimum balance between sensitivity and noise immunity.

This switch to continuum-free infrared ArI lines seems a far better move than use of any of several experimental and theoretical procedures which could be used to overcome the obstacle of strong visible continuum radiation from short-standoff PAW plasma. It is a well-established, accurate approximation that argon (but not helium) plasma is in local thermodynamic equilibrium for current densities of welding interest and at pressures near one

atmosphere.[7,14] This means both that local temperature can be measured (with the accuracy we require) by the two-line method, and that it can be measured equally well with ArI (neutral argon) lines or with ArII (singly-ionized argon) lines. Alternate procedures, retianing use of the visible ArII lines, would pose serious experimental or theoretical difficulties. For example, by use of additional beam splitters and narrow bandpass filters, the plasma could be photographed simultaneously--still from two directions--by the emission of two spectral lines plus continuum radiation of the same wavelength, and by the emission of continuum radiation alone at nearby line-free wavelengths. This would permit complete spatial resolution of the continuum radiation at two line-free wavelengths, and by interpolation, at the wavelengths of the lines of interest. Point-by-point, rather than mean-fractional, correction of the line emissivities could then be made. Then, however, temperature calculations would be based on line emissivity found as the somewhat small difference (about 30% as observed to date) of larger quantities, one of which would be known only by interpolation procedure. Another possible approach is to use theoretical estimates of the relative emissivities of continuum (free-free and free-bound electronic transitions) and spectral line (bound-bound transitions) within the filter passband. However, this apparently would lead to an equation for the temperature which is much more difficult to solve than Eq. (7)--it would be an implicit rather than an explicit function of the observable intensities--and also is less reliable. The theory of continuum radiation is not as well worked out as that of line radiation, and is less accurate.[14] Moreover, an important advantage of the two-line method of temperature measurement--insensitivity to the presence of impurities in the plasma--would be lost.

In addition to use of the ArI lines, for which the necessary interference filters have already been obtained, further automation of image analysis and data reduction will be implemented. A quadratically-convergent method for finding the optimum value of the scale factor will be used to speed computation. Temperature distributions will be generated systematically and correlated with eight welding parameters (travel speed, current, standoff, orifice diameter, electrode diameter, electrode taper, setback, and gas flow) on the one hand, and with visual, metallurgical and mechanical weld quality on the other hand.

5.0 REFERENCES

1. Interim report, AFML Contract F33615-74-C-5036, "Manufacturing Methods for Plasma Arc Welding," Rockwell International, El Segundo, Calif., 1974 and 1975.

2. P. Demars, J. P. Schultz, F. Cuny, "Les Nouvelles Possibilités du Procédé Plasma en Soudage," Soudages et Techniques Connexes 5/6, 211-230 (1973).

3. H. N. Olsen, "Thermal and Electrical Properties of High Current Argon Arc Plasmas," Eleventh Annual Gaseous Electronics Conference, October 22-25, 1958, New York. (The spectroscopic technique applied in this paper had been described at the previous year's Conference.)

4. H. N. Olsen, C. D. Maldonado and G. D. Duckworth, "A Numerical Method for Obtaining Internal Emission Coefficients from Externally Measured Spectral Intensities of Asymmetrical Plasma," J. Quant. Spectrosc. Radiat. Transfer 8, 1419-1430 (1968).

5. H. N. Olsen, private communication, 1971.

6. C. D. Maldonado and H. N. Olsen, "New Method for Obtaining Emission Coefficients from Emitted Spectral Intensities. Part II--Asymmetrical Sources," J. Opt. Soc. Am. 56, 1305-1313 (1966).

7. W. Lochte-Holtgreven, "Evaluation of Plasma Parameters," Chapter 3 of Plasma Diagnostics, W. Lochte-Holtgreven, ed. (John Wiley & Sons, New York, 1968).

8. C. B. Shaw, Jr., "Improvement of the Resolution of an Instrument by Numerical Solution of an Integral Equation," J. Math. Anal. Appl. 37, 83-112 (1972).

9. C. B. Shaw, Jr., "Best Accessible Estimation: Convergence Properties and Limiting Forms of the Direct and Reduced Versions," J. Math. Anal. Appl. 44, 531-552 (1973).

10. C. B. Shaw, Jr. and B. I. Davis, "Time-Resolved Temperature and Density Distribution in a Welding Arc," IEEE International Conference on Plasma Science, Knoxville, Tennessee, May 15-17, 1974. Conference Record IEEE publication 74CH0922-5-NPS.

11. C. B. Shaw, Jr., "Diagnostic Studies of the GTAW Arc," selected for presentation at 54th Annual Meeting, American Welding Society, Chicago, April 2-6, 1973; Welding Journal 54, 33s-44s and 73s-80s (1975).

12. C. B. Shaw, Jr., "Reconstruction from a Few Imperfect Projections," invited paper presented at International Workshop on Three-Dimensional Image Reconstruction Techniques sponsored by National Science Foundation at Brookhaven National Laboratory, July 15-19, 1974. Proceedings published as BNL 20425.

13. C. B. Shaw, Jr. and B. I. Davis, "Diagnostic Arc Studies with Ruby Laser," Proc. Soc. Photo-Optical Instr. Eng. 41, 89-99 (1973).

14. J. Richter, "Radiation of Hot Gases," Chapter 1 of Plasma Diagnostics, W. Lochte-Holtgreven, ed. (John Wiley & Sons, New York, 1968).